Chunguang Chen,[1,2,3] Helena Chmelova,[1,2,3] Christian M. Cohrs,[1,2,3] Julie A. Chouinard,[1,2,3] Stephan R. Jahn,[1,2,3] Julia Stertmann,[1,2,3] Ingo Uphues,[4] and Stephan Speier[1,2,3]

Alterations in β-Cell Calcium Dynamics and Efficacy Outweigh Islet Mass Adaptation in Compensation of Insulin Resistance and Prediabetes Onset

Diabetes 2016;65:2676–2685 | DOI: 10.2337/db15-1718

ISLET STUDIES

Emerging insulin resistance is normally compensated by increased insulin production of pancreatic β-cells, thereby maintaining normoglycemia. However, it is unclear whether this is achieved by adaptation of β-cell function, mass, or both. Most importantly, it is still unknown which of these adaptive mechanisms fail when type 2 diabetes develops. We performed longitudinal in vivo imaging of β-cell calcium dynamics and islet mass of transplanted islets of Langerhans throughout diet-induced progression from normal glucose homeostasis, through compensation of insulin resistance, to prediabetes. The results show that compensation of insulin resistance is predominated by alterations of β-cell function, while islet mass only gradually expands. Hereby, functional adaptation is mediated by increased calcium efficacy, which involves Epac signaling. Prior to prediabetes, β-cell function displays decreased stimulated calcium dynamics, whereas islet mass continues to increase through prediabetes onset. Thus, our data reveal a predominant role of islet function with distinct contributions of triggering and amplifying pathway in the in vivo processes preceding diabetes onset. These findings support protection and recovery of β-cell function as primary goals for prevention and treatment of diabetes and provide insight into potential therapeutic targets.

Obesity and insulin resistance are important risk factors for type 2 diabetes (T2D) (1). However, the majority of obese and insulin-resistant subjects do not develop hyperglycemia (2). This is attributed to the compensatory capacity of the islets of Langerhans, which meet the increased insulin demand by an elevated hormone output (3). Two processes have been implicated in islet compensation in response to obesity and insulin resistance: First, an increased functionality and insulin secretion rate of the individual β-cells, e.g., by enhancing glucose metabolism or insulin gene expression or translation (4–6). In addition, increased systemic insulin output can be achieved by a morphological enlargement of β-cell mass through proliferation (7,8), hypertrophy (5,8), or neogenesis (9,10). Whereas in rodents β-cell mass has been reported to increase substantially in response to insulin resistance (7,11), this seems to be less pronounced in humans (12–14).

Failure of β-cell compensation in insulin resistance and obesity is believed to be a cause of T2D. Both altered β-cell function and mass have been suggested to contribute to hyperglycemia. Decreased β-cell function was observed in islets isolated from organ donors with T2D (15) and animal models (16). In addition, rodent T2D models were shown to exhibit a reduction in β-cell mass (11,17–19). Data on alterations of β-cell mass in humans with T2D are inconsistent and vary from no significant changes up to a 63% decrease in comparison with subjects without diabetes (12,14,20,21). However, the relative contribution of β-cell mass and function to the maintenance of normoglycemia in insulin resistance and their distinct roles in the onset of insulin deficiency and hyperglycemia are unclear. It remains elusive whether the observed β-cell changes in T2D patients and hyperglycemic animal models are cause

[1]Paul Langerhans Institute Dresden, Helmholtz Center Munich, University Clinic Carl Gustav Carus, Technische Universität Dresden, Helmholtz Zentrum München, Neuherberg, Germany
[2]German Research Foundation–Center for Regenerative Therapies Dresden (CRTD), Faculty of Medicine, Technische Universität Dresden, Dresden, Germany
[3]German Center for Diabetes Research (DZD), München-Neuherberg, Germany
[4]Boehringer Ingelheim Pharma GmbH & Co. KG, Ingelheim, Germany
Corresponding author: Stephan Speier, stephan.speier@tu-dresden.de.

Received 17 December 2015 and accepted 5 April 2016.

This article contains Supplementary Data online at http://diabetes.diabetesjournals.org/lookup/suppl/doi:10.2337/db15-1718/-/DC1.

See accompanying article, p. 2470.

or consequence of the altered glucose homeostasis. To a large degree this is due to the inability to separately assess β-cell mass and function in vivo.

In this study, we monitored for the first time in vivo dynamics and mechanisms of islet and β-cell mass in relation to systemic glucose homeostasis during long-term diet-induced obesity and insulin resistance. This allowed us to assess the kinetics and relative contribution of β-cell mass during the compensation phase and prediabetes stage of diabetes pathogenesis. Our results show that the functional response of β-cells dominates over islet mass adjustment in compensation of insulin resistance and during the development of prediabetes. To study the underlying mechanism of functional adaptation, we monitored intracellular calcium (Ca^{2+}_i) dynamics of β-cells longitudinally in vivo. This revealed increased calcium efficacy as a crucial adaptive mechanism of β-cell function, which was dependent on Epac signaling in isolated islets. Meanwhile, Ca^{2+}_i dynamics in vivo showed an early decline preceding the onset of prediabetes. Therefore, our study provides novel insight into the pathogenesis of T2D and potential therapeutic targets.

RESEARCH DESIGN AND METHODS

Mice

All experiments were conducted in accordance with the German Animal Welfare Act and approved by the Committee on the Ethics of Animal Experiments of the State Directory of Saxony. C57BL/6N albino mice (B6N-$^{Tyrc\text{-}Brd}$/BrdCrCrl; Charles River Laboratories) were used as recipients for islet transplantation. Mice expressing green fluorescent protein under control of the mouse insulin I promoter (MIP-GFP) (22) and Pdx1CreER-GCaMP3 mice, both on C57Bl/6J background (The Jackson Laboratory), were used as islet donors. Pdx1CreER-GCaMP mice were generated by crossing Pdx1CreER mice (23) with homozygous GCaMP3 mice (The Jackson Laboratory) (24). For induction of β-cell–specific GCaMP3 protein expression, Pdx1CreER-GCaMP3 mice were injected with tamoxifen (3 × 4 mg s.c. in corn oil over 5 days) 2 weeks before islet isolation.

Diet-Induced Obesity Model

Recipient mice received either standard normal diet (ND) (ssniff) or rodent high-fat diet (HFD) with 60% of kcal as fat (D12492; Research Diets) for 17 weeks before switching back to ND in the HFD group. Body weight and intraperitoneal glucose tolerance tests (IPGTTs) were assessed at indicated time points. For IPGTTs, mice were fasted for 6 h and injected with 2 g glucose/kg body wt i.p. Blood glucose was measured at 0, 30, 60, and 120 min after glucose injection using a glucometer (Accu-Chek Aviva, Roche). Plasma insulin was measured at 0 and 30 min using a mouse Ultrasensitive Insulin ELISA kit (ALPCO). Prediabetes was defined as significantly increased 2-h blood glucose values at unchanged nonfasting blood glucose levels.

Islet Isolation, Transplantation, and In Vivo Imaging of Islet and β-Cell Volume

Islet isolation and transplantation to the anterior chamber of the eye were performed as previously described (25–28). Transplanted islets were allowed to engraft fully for at least 4 weeks before the start of any in vivo experiments. In vivo imaging was performed as previously described (26). Briefly, islet recipients were intubated and anesthetized by 2% isoflurane in 100% oxygen. A drop of 0.4% pilocarpine (Pilomann; Bausch & Lomb, Rochester, NY) in saline was placed on the cornea shortly before imaging to limit pupil dilation and iris movement. Animals were fixated and kept on a heating pad during the imaging procedure. Repetitive in vivo imaging was performed at indicated time points on an upright laser scanning microscope (LSM780 NLO; Carl Zeiss, Jena, Germany) with a water dipping objective (W Plan-Apochromat 20×/1.0 DIC M27 75 mm; Carl Zeiss) using vidisic eye gel (Bausch & Lomb) as immersion. The total volume of transplanted islets was assessed by detection of 633 nm laser backscatter, which allows assessment of islet morphology based on its light-scattering properties (27). Total volume of each islet was calculated using surface rendering after three-dimensional reconstruction of collected image stacks (Imaris 7.6; Bitplane AG, Zurich, Switzerland). β-Cell volume in MIP-GFP islets was assessed by two-photon laser excitation of GFP at 910 nm and detection at 500–550 nm using a nondescanned gallium arsenide phosphate detector. β-Cell volume was then quantified by automatic surface rendering from median filtered Z stacks in Imaris 7.6 (Bitplane AG). Qtracker 655 (0.4 μmol/L in 100 μL PBS; Life Technologies) was injected into the tail vein to visualize blood vessels. Qtracker were excited by two-photon laser at 910 nm and detected at 635–675 nm. Vessel volume was calculated by automatic surface rendering. Vessel network length and vessel diameter were measured by filament tracing within the vessel surface using Imaris software.

In Vivo Imaging of β-Cell Cytosolic Free Calcium Dynamics

Pdx1CreER-GCaMP3 islet recipient mice were fasted overnight and anesthetized with an injection of a mixture of fluanisone (12.5 μg/g body wt i.p.; CHEMOS, Regenstauf, Germany), fentanyl (0.788 μg/g body wt i.p.; Hameln Pharma Plus, Hameln, Germany), and midazolam (12.5 μg/g body wt i.p.; Ratiopharm, Ulm, Germany). The anesthetized mice were intubated and respiration was maintained by use of a small animal ventilator with room air (270 μL stroke volume, 250 strokes/min; Hugo Sachs, March-Hugstetten, Germany). Animals were fixed and positioned as described above. In vivo imaging was performed using confocal laser scanning microscopy. The volume of islets was assessed by detection of 633 nm backscatter laser light. The functional index of islets was calculated by dividing stimulated plasma insulin by fold changes in islet mass at corresponding time points in the same mice.

GCaMP3 GFP was excited at 488 nm and detected at 468–607 nm. Z stacks of the islet were acquired at 1.5-μm intervals, and time-series recording of GCaMP3 GFP signal from the same islets was carried out with an image sampling rate of 2 s. After acquisition of a baseline recording for 5 min, glucose was injected (1 g/kg body wt i.v.) via the tail vein. Changes in β-cell $Ca^{2+}{}_i$, as reflected by changes in GCaMP3 GFP fluorescence intensity, were recorded for 30 min after glucose injection. After the recording, mice were maintained on ventilator breathing until autonomous respiration was restored. Z stacks and time series were processed using Imaris 8.1 software (Bitplane AG). The GCaMP3-expressing β-cell area was defined by applying a threshold acquired in the GFP-negative area. Mean GCaMP3 GFP fluorescence per β-cell area was calculated for each frame and normalized to the minimal value in the baseline. Finally, total β-cell $Ca^{2+}{}_i$ dynamics was quantified by calculating the area under the curve of the fluorescence trace for 5 min before glucose injection (basal $Ca^{2+}{}_i$ dynamics) and 30 min after glucose injection (stimulated $Ca^{2+}{}_i$ dynamics). In vivo calcium efficacy was calculated by dividing stimulated plasma insulin by the product of stimulated $Ca^{2+}{}_i$ dynamics per minute and fold changes in islet mass at corresponding time points in the same mice. First-phase peak amplitude was defined by the peak intensity over mean basal intensity within 5 min after glucose injection.

In Vitro Culture and Insulin Secretion

After overnight culture in standard RPMI 1640 medium, islets from female C57Bl/6J mice were handpicked and cultured in 24-well plates in culture medium with a 0.1 mmol/L BSA, 8 mmol/L glucose, and 0.5 mmol/L BSA–conjugated palmitate ($G_8P_{0.5}$). Control islets were cultured in RPMI 1640 media in the presence of 5.5 mmol/L glucose without palmitate ($G_{5.5}P_0$). The Epac-specific inhibitor ESI-09 (1–5 μmol/L; Sigma-Aldrich) was applied in both basal culture and during glucose stimulated insulin secretion when indicated. Basal insulin secretion was assessed from 24-h culture medium and corrected for release per hour. For assessment of stimulated insulin release, islets were placed for 1 h in their respective culture medium, containing elevated glucose concentrations (25 mmol/L). Islets were lysed in acid/ethanol buffer for insulin content. Total insulin content was defined by the sum of insulin secreted into medium upon stimulation and insulin content in the lysate. Collected medium and islet lysate were stored at −20°C until insulin content was measured using a mouse Ultrasensitive Insulin ELISA kit (ALPCO).

In Vitro Imaging of β-Cell Cytosolic Free Calcium Dynamics

For in vitro imaging of cytosolic free calcium dynamics in β-cells, Pdx1CreER-GCaMP islets were handpicked after overnight culture and embedded in fibrin gels on coverslips according to a previously published protocol (29). Briefly, fibrin gels were prepared by mixing 3 μL Hanks' balanced salt solution (HBSS) with 1 μL human fibrinogen (10 mg/mL in HBSS; Sigma-Aldrich), after which six islets were placed individually in the gel. Fibrinogen polymerization was induced by adding 1 μL human thrombin (50 units/mL in HBSS; Sigma-Aldrich). Subsequently, the gel-embedded islets were cultured for 24 h in indicated conditions. Calcium imaging was performed in a custom-made perifusion system (30). Briefly, coverslips with gel-embedded islets were moved into a temperature-controlled perifusion chamber where the temperature was set at 37°C. In vitro imaging was performed in the above-described laser scanning microscope system. GCaMP3 GFP was excited at 488 nm and detected at 493–598 nm. Time-series recording of the GCaMP3 GFP signal from the same islets was carried out with an image-sampling rate of 2 s. A basal recording was acquired for 3 min when the islets were perifused in their respective culture medium. For stimulation, islets were perifused with their respective culture medium, containing elevated glucose concentrations (25 mmol/L). Changes in β-cell $Ca^{2+}{}_i$ were recorded for 25 min after stimulation. Mean GCaMP3 GFP fluorescence per β-cell area and total β-cell GCaMP3 GFP fluorescence was processed and quantified using the same protocol as for the in vivo imaging. Basal and stimulated $Ca^{2+}{}_i$ dynamics are displayed as area under the curve per minute in basal and stimulated conditions, respectively. Calcium efficacy was calculated by dividing stimulated insulin by stimulated $Ca^{2+}{}_i$ dynamics per minute in corresponding experiments.

Pancreatic β-Cell Area

Fractional pancreatic β-cell area was assessed in cryosections (10 μm) stained for insulin (1:200 dilution; Dako, Hamburg, Germany), glucagon (1:500; Merck Millipore, Darmstadt, Germany), and DAPI (2.5 μg/L; Sigma-Aldrich). Immunostaining was visualized by Alexa Fluor 488 and Alexa Fluor 633 secondary antibodies (1:200; Life Technologies). Images were acquired in a slide scanner (Axio Scan.Z1; Carl Zeiss). Quantification of immunohistochemistry was done manually using Fiji software. Fractional β-cell area was calculated from at least 40 pancreas sections (with a minimal distance of 150 μm between sections) per mouse.

Statistical Analysis

Data are expressed as mean ± SEM. Statistics were analyzed using Prism 6 (GraphPad Software, San Diego, CA) or SPSS 21 (IBM, Armonk, NY). For proper acknowledgment of the two sources of correlation that are inherent to the repeated longitudinal measurements, longitudinal in vivo data were analyzed by linear mixed models (26). Significant differences are indicated at $P < 0.05$.

RESULTS

HFD Induces Impaired Glucose Tolerance and Prediabetes Despite the Compensational Release of Insulin

We transplanted reporter islets for in vivo imaging into the anterior chamber of the eye of albino C57Bl/6N mice. After engraftment, recipient mice were fed with ND (11% kcal

from fat) or HFD (60% kcal from fat) for 17 weeks, followed by 2 weeks of ND. HFD mice showed continuously increasing body weight (37.3 ± 0.6 vs. 26.2 ± 0.5 g for HFD vs. ND, respectively, at 17 weeks) (Fig. 1*A*). Furthermore, fasting blood glucose levels were slightly, but significantly, increased at several time points during the study (Fig. 1*B*). Fasting and stimulated plasma insulin levels in response to an IPGTT increased during HFD, reaching a plateau at 9 weeks (fasting 0.68 ± 0.11 vs. 0.16 ± 0.06 ng/mL for HFD vs. ND at 9 weeks; stimulated 1.28 ± 0.16 vs. 0.34 ± 0.06 ng/mL for HFD vs. ND at 9 weeks) (Fig. 1*C* and *D*). Also, the fasting and stimulated plasma insulin levels in relation to the given glucose concentration were increased in HFD, indicating an increased sensitivity of β-cells to glucose (Fig. 1*E* and *F*). However, despite the elevated insulin release, glucose tolerance continuously deteriorated in HFD mice (Fig. 1*G*). In addition, the 2-h glucose tolerance test value was significantly higher after 9 weeks of HFD feeding, indicating a stage of prediabetes in these animals (Fig. 1*H*).

Islet and β-Cell Mass Gradually Increases in Response to HFD

Islets engrafted in the anterior chamber of the eye of the above-described mice allowed longitudinal assessment of total islet volume by backscatter laser light during long-term ND and HFD feeding. The acquired backscatter volume included all endocrine cells and the vascular network of an islet (Fig. 2*A* and *B*). While the total volume of islets in ND-fed mice remained unchanged, islets within HFD-fed mice showed a slow but continuous increase in size, doubling in volume after 16 weeks of HFD exposure (1.97 ± 0.14-fold vs. 1.07 ± 0.08-fold increase for HFD vs. ND at week 16) (Fig. 2*A* and *C*).

Using MIP-GFP reporter islets in the anterior chamber of the eye during HFD demonstrated that the observed islet mass enlargement was due to β-cell expansion (1.88 ± 0.17-fold increase at week 16) (Fig. 3*A* and *B*). This was the result of an increase in β-cell number (1.92 ± 0.15-fold increase at week 16) (Fig. 3*C*), whereas no significant change in the individual β-cell size was observed (Fig. 3*D*). Intraislet vessels adapted to islet growth and contributed to total islet volume increase by a lengthening of the vascular network (2.11 ± 0.15-fold increase at week 16) (Fig. 3*A* and *E*), thereby maintaining a constant fractional vessel volume within the growing islets (data not shown). In addition, intraislet vessel diameter increased in response to HFD presumably to match the increased secretory activity (8.79 ± 0.09 vs. 8.22 ± 0.11 μm for HFD vs. ND at week 16) (Fig. 3*F*). Pancreatic β-cell area showed a similar, circa twofold, increase after 16 weeks of HFD feeding in our setting (Fig. 3*G* and Supplementary Fig. 1), verifying the validity of the anterior chamber of the eye platform to study islet biology during HFD.

Because the kinetics of islet mass expansion (Fig. 2*C*) and rising plasma insulin levels (Fig. 1*D*) within the same animal showed obvious differences, we calculated an approximate index of the relative contribution of β-cell function by dividing stimulated plasma insulin by the increase in islet cell mass. β-Cell functional index peaked

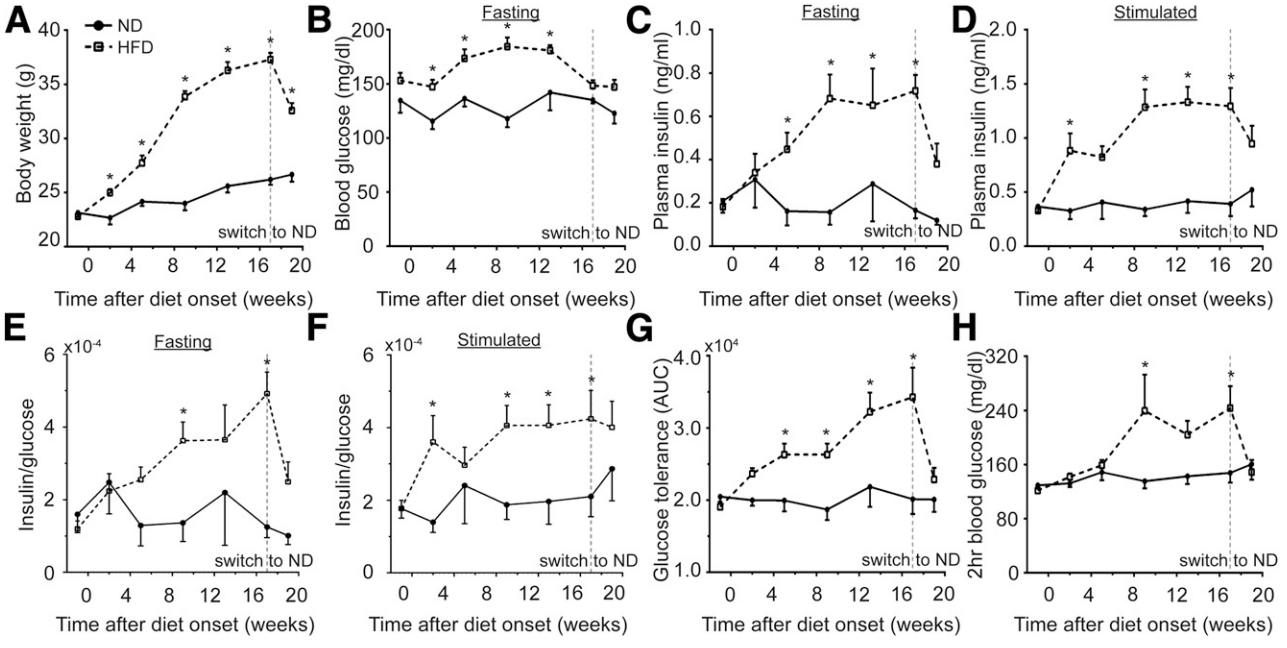

Figure 1—HFD leads to impaired glucose tolerance and prediabetes despite increased insulin secretion. Effect of 17 weeks of ND or HFD feeding, followed by 2 weeks of ND, on body weight (*A*), fasting blood glucose (*B*), fasting insulin (*C*), stimulated insulin (*D*), insulin-to-glucose ratio in fasting (*E*) and stimulated (*F*) state during IPGTT, glucose tolerance (*G*), and 2-h glucose tolerance blood glucose levels (*H*). n = 3–8 for ND and 6–8 for HFD. Mean ± SEM. *P < 0.05 vs. ND. AUC, area under the curve; hr, hour.

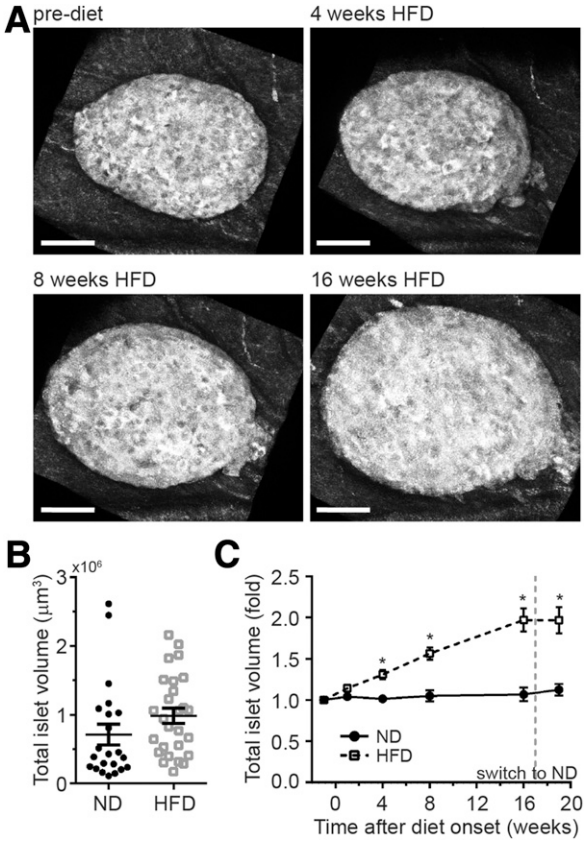

Figure 2—Prolonged HFD feeding induces a continuous increase of islet volume. *A*: In vivo backscatter images of a representative islet engrafted in the anterior chamber of the eye of a mouse at indicated time points during HFD feeding. *B*: Islet volume (quantified by laser backscatter [μm^3]) of individual islets at the initial time point (prediet). *C*: Total islet volume (quantified by laser backscatter [fold change]) of intraocular islets during prolonged ND and HFD feeding. n = 11–27 islets in 3–8 mice; mean ± SEM. *$P < 0.05$ vs. ND. Scale bars: 50 μm.

within 1 week of HFD feeding with a threefold increase over ND (3.2 ± 1.0 vs. 1.1 ± 0.2 for HFD vs. ND) (Fig. 4). Thereafter, it remained elevated over ND throughout the HFD feeding period at slightly reduced levels (2.6 ± 0.6-fold, 2.8 ± 0.3-fold, and 2.5 ± 0.5-fold at weeks 4, 8, and 16, respectively) (Fig. 4). This revealed that β-cell function showed an immediate strong compensatory response to HFD feeding, which in contrast to islet mass did not further increase during the course of prediabetes development.

β-Cell Functional Adaptation to HFD Is Associated With Increased Basal and Decreased Glucose-Stimulated Ca^{2+}_i

We examined the role of Ca^{2+}_i dynamics in the functional compensation of β-cells during prolonged HFD feeding by longitudinal in vivo imaging. To this end, we transplanted Pdx1CreER-GCaMP3 islets into albino C57Bl/6N mice. Prior to islet isolation and transplantation, CreER-LoxP–mediated recombination of GCaMP3 expression was induced by tamoxifen application to the islet donor. As previously reported in neurons (24), Ca^{2+}_i dynamics in β-cells was assessed by monitoring GFP fluorescence of the GCaMP3 reporter in response to an intravenous glucose challenge at indicated time points before, during, and after long-term ND or HFD feeding (Fig. 5). Under control conditions, β-cells showed little or no basal Ca^{2+}_i dynamics (Fig. 5*A*, panel 1). Upon glucose injection into the tail vein of the recipient mouse, β-cells displayed a strong peak of Ca^{2+}_i dynamics (Fig. 5*A*, panel 2), followed by a lower plateau and/or oscillations in Ca^{2+}_i (Fig. 5*A*, panels 3–5). Islets displayed a continuous plateau, regular oscillations, or a mix of both after the initial peak. The respective pattern of Ca^{2+}_i dynamics of an islet was comparable at the various recording time points and was synchronized throughout the image plane. Islets in ND mice showed few alterations in Ca^{2+}_i dynamics during repetitive imaging over 19 weeks (Fig. 5*B*). However, in response to HFD feeding GCaMP3 GFP fluorescence traces displayed considerable changes in basal and stimulated Ca^{2+}_i dynamics (Fig. 5*C*).

Quantification revealed that minimum values of GCaMP3 GFP fluorescence intensity were comparable between islets in ND and HFD mice throughout the study. This suggests that there were no major changes in expression of the fluorescent reporter or resting Ca^{2+}_i levels. However, basal islet Ca^{2+}_i dynamics, assessed as area under the curve of the GCaMP3 GFP fluorescence trace prior to intravenous glucose injection, continuously increased in islets of the HFD-fed mice (7.93 ± 0.45 vs. 6.25 ± 0.27 arbitrary units for HFD vs. ND at week 16) (Fig. 6*A*). This parallels the observed rising levels of basal plasma insulin (Fig. 1*C*), which are most likely the result of elevated basal glucose levels (Supplementary Fig. 2*A*) and increasing glucose sensitivity (Fig. 1*E*). In contrast, stimulated Ca^{2+}_i dynamics in response to intravenous glucose decreased early and remained significantly lower in the HFD group (42.05 ± 2.32 vs. 52.83 ± 2.60 arbitrary units for HFD vs. ND at week 16) (Fig. 6*B*). This was associated with a reduced first-phase peak amplitude of calcium activity after glucose injection (Fig. 6*C*), while second-phase oscillation amplitude and frequency were highly variable among islets of both groups and showed no significant effect by HFD feeding. Increased β-cell function without elevation in stimulated Ca^{2+}_i dynamics suggested an augmentation of insulin release by amplification of calcium-induced secretion in vivo to overcome impaired glucose tolerance (Fig. 1*G* and Supplementary Fig. 2*B*). This was illustrated by the calculated enhanced efficacy of calcium to induce insulin release during HFD feeding (Fig. 6*D*).

Inhibition of Epac Signaling Blocks Amplified Calcium Efficacy

To reveal the mechanism underlying amplified calcium efficacy, we mimicked the acute functional compensation by 24-h culture of isolated mouse islets in 8 mmol/L glucose plus 0.5 mmol/L palmitate ($G_8P_{0.5}$). This condition resembled the slightly elevated glucose levels and the

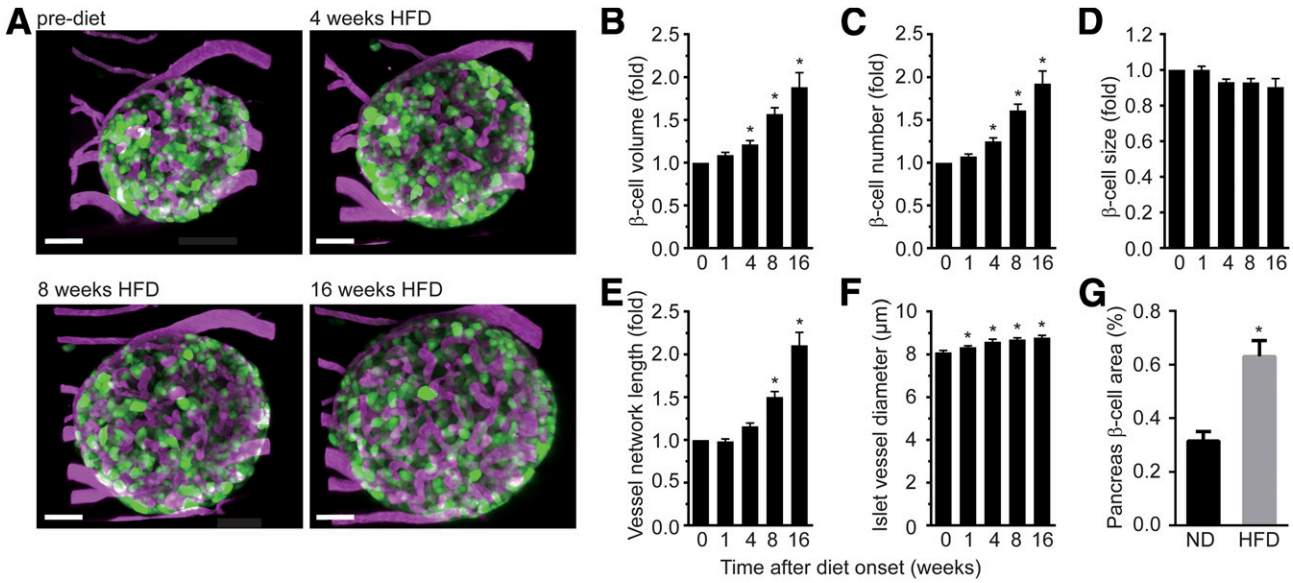

Figure 3—HFD-induced islet growth is the result of increased β-cell number and vessel network adaptation. *A*: In vivo fluorescence images of an intraocular MIP-GFP islet at indicated time points of HFD feeding (green, MIP-GFP; magenta, vessels). *B–F*: Longitudinal effect of HFD feeding on β-cell volume (*B*), number (*C*), and size (*D*), as well as on islet vessel network length (*E*) and diameter (*F*). n = 18–33 islets in 4–7 mice; mean ± SEM. **P* < 0.05 vs. prediet. Scale bars: 50 μm. *G*: Fractional β-cell area (percentage of total pancreatic area) of mice with ND or 16 weeks of HFD feeding. n = 6 mice; mean ± SEM. **P* < 0.05 vs. ND.

presence of increased free fatty acids observed during HFD in vivo. The control islets were cultured in $G_{5.5}P_0$ to resemble ND feeding. Compared with control, $G_8P_{0.5}$ islets had significantly higher basal and glucose-stimulated insulin secretion (Fig. 7*A*). At the same time, $G_8P_{0.5}$ islets showed significantly higher basal $Ca^{2+}{}_i$ dynamics in vitro, while glucose-stimulated $Ca^{2+}{}_i$ dynamics was slightly but significantly reduced (Fig. 7*B*). This revealed a significantly higher calcium efficacy of $G_8P_{0.5}$ islets upon stimulation (Fig. 7*C*), identical to what we observed during HFD in vivo (Fig. 6*D*). Previous data indicate cAMP mediated signaling via the exchange protein activated by cAMP (Epac) to potentiate insulin secretion and mediate the β-cell response to increased metabolic demand (31,32). We therefore assessed the role of Epac in the observed elevated calcium efficacy in our conditions. ESI-09, an Epac-specific inhibitor, dose-dependently (1, 3, and 5 μmol/L) reduced glucose-stimulated insulin secretion when supplemented in $G_8P_{0.5}$ islet culture and stimulation, while basal insulin secretion was not significantly affected (Fig. 7*D*). On the other hand, 5 μmol/L ESI-09 had no effect on basal or stimulated calcium dynamics (Fig. 7*E*), revealing a significant inhibition of calcium efficacy by 5 μmol/L ESI-09 (Fig. 7*F*) and indicating a crucial role of Epac in the amplification of insulin secretion by increased calcium efficacy.

Changes in Glucose Homeostasis and β-Cell Function Are Reversed by ND Feeding

Interestingly, after 17 weeks of HFD, a subsequent 2-week period of ND was sufficient to reverse the observed phenotype. Body weight decreased but remained significantly elevated (Fig. 1*A*). Fasting blood glucose and glucose tolerance returned to control values (Fig. 1*B*, *G*, and *H*). Also, basal and stimulated plasma insulin levels dropped markedly (Fig. 1*C* and *D*). Furthermore, islet mass enlargement stopped when HFD mice were switched back to ND (Fig. 2*C*). Finally, β-cell functional index (Fig. 4) as well as basal and stimulated calcium dynamics (Fig. 6*A* and *B*) was restored to prediet values.

DISCUSSION

In our study, we assessed for the first time islet mass and β-cell function longitudinally throughout the progression from normal glucose tolerance, through compensation, to prediabetes. For this purpose, we correlated systemic glucose

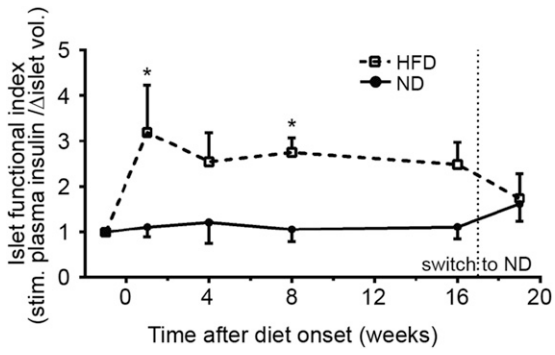

Figure 4—Islets compensate HFD feeding with an increased β-cell functional index. Islet functional index, calculated as stimulated (stim.) plasma insulin levels over total islet volume (vol.) adaptation of the same animal. n = 9–24 islets in 3–8 mice; mean ± SEM. **P* < 0.05 vs. ND.

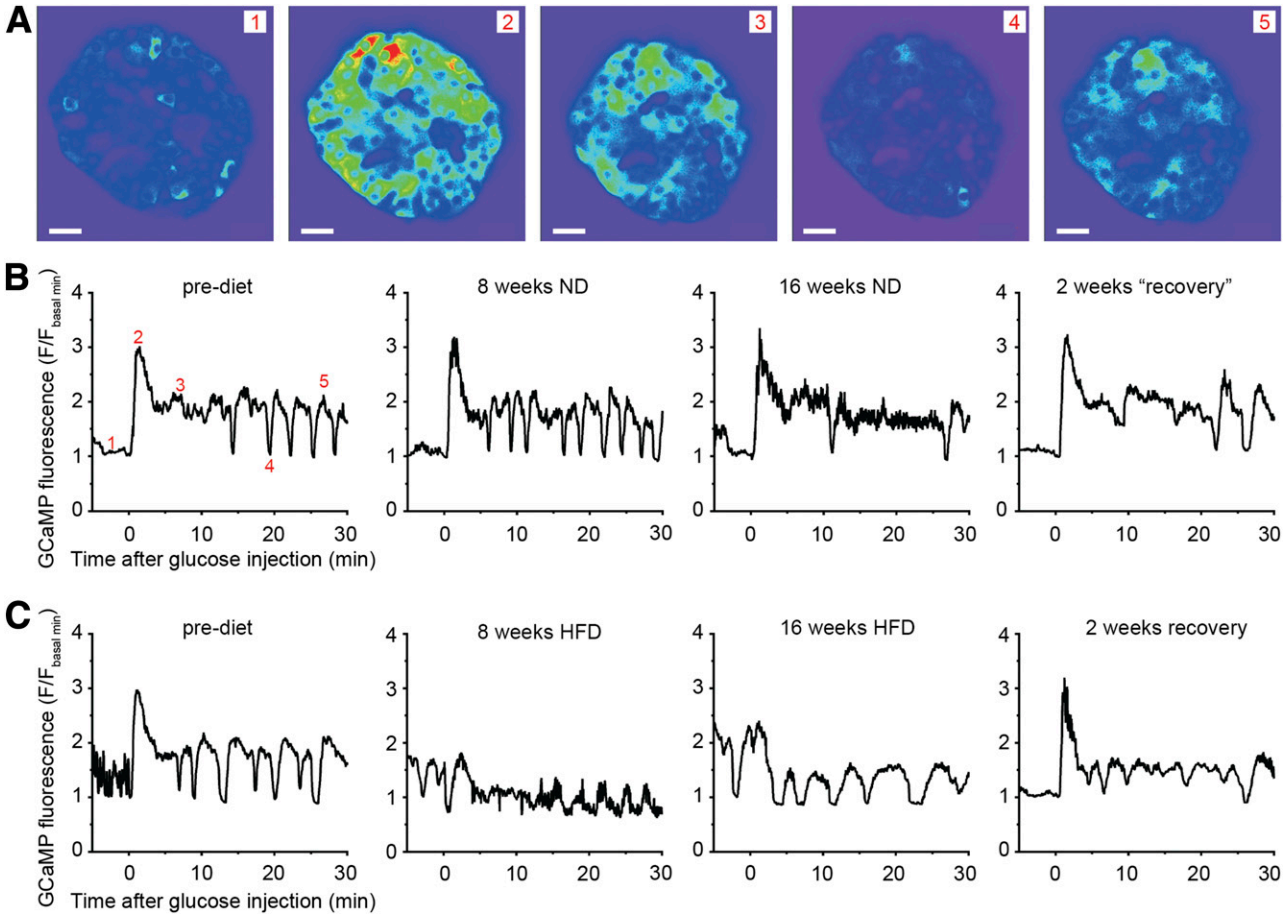

Figure 5—Longitudinal in vivo imaging of β-cell Ca^{2+}_i dynamics during prolonged ND and HFD feeding. *A*: Intensity-encoded images from indicated time points of the Pdx1CreER-GCaMP3 islet GFP fluorescence recording shown in *B* (prediet). Scale bars: 20 μm. *B* and *C*: Representative repetitive recordings of in vivo Ca^{2+}_i dynamics of a Pdx1CreER-GCaMP3 islet in response to an intravenous glucose injection (0 min) at indicated time points during 17 weeks of ND (*B*) or HFD (*C*) feeding and after a subsequent 2 weeks on ND (recovery).

homeostasis with longitudinal in vivo imaging of transplanted islets of Langerhans during diet-induced obesity. Although we cannot exclude potential effects of the different local environment on intraocular islets, our own data and previous studies suggest that the behavior of islets in the anterior chamber of the eye closely resembles that of endogenous pancreatic islets (26,28,33–35).

Our results reveal that HFD feeding, a model of early diabetes pathogenesis (36), leads to distinct dynamics of β-cell mass and function preceding the onset of diabetes. Initially, enhanced β-cell function compensates insulin resistance by elevated plasma insulin levels in the absence of any significant islet mass increase. During a second phase, gradual islet mass expansion contributes to rising plasma insulin levels in combination with elevated β-cell function. However, despite a continuous islet mass increase, ongoing HFD feeding subsequently leads to prediabetes as a result of insufficient β-cell function. In our study, islet mass is not decreased at the time of prediabetes onset but, on the contrary, is still increasing. This supports the hypothesis that β-cell function and not islet mass decline is the crucial islet-related mechanism in early T2D pathogenesis. This is in line with the observation that the majority of known T2D susceptibility genes are associated with β-cell function (37). Therefore, observed reduced β-cell mass in individuals with T2D might be a result of stress-induced cell death or dedifferentiation after onset of hyperglycemia (20). However, our results do not rule out a potential role of β-cell mass at later stages of diabetes pathogenesis or the influence of diminished inherent β-cell mass for diabetes development (38).

In our investigation of the mechanisms underlying functional compensation, our findings suggest that increasing fasting plasma insulin levels in HFD are the result of enhanced β-cell function illustrated by the rising basal Ca^{2+}_i dynamics. Higher fasting insulin has also been observed in other mouse models of T2D (39) and is most likely due to an increased glucose sensitivity of β-cells in the presence of elevated free fatty acid levels (40). Conversely, whereas plasma insulin levels were increased in response to glucose, we found stimulated Ca^{2+}_i dynamics to be reduced under HFD in vivo, which was associated with a decreased first-phase response. In dispersed cells or isolated islets, diminished stimulated Ca^{2+}_i dynamics was

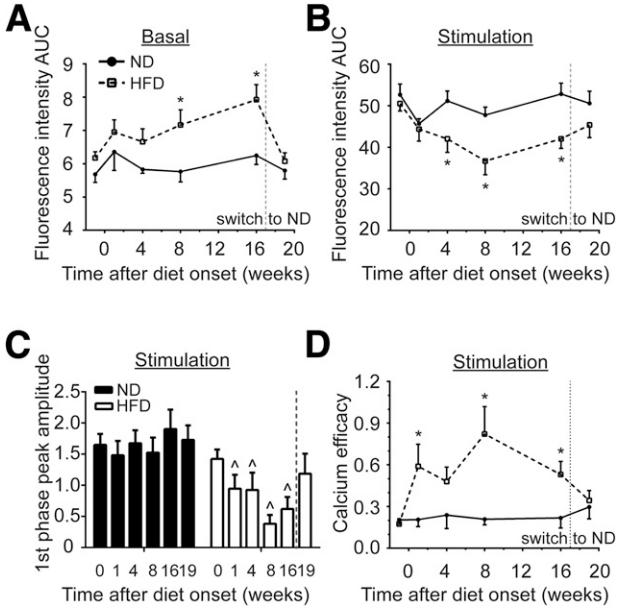

Figure 6—HFD induces increased basal and decreased glucose-stimulated β-cell Ca^{2+}_i dynamics in vivo. *A* and *B*: Quantification of basal (*A*) and stimulated (*B*) β-cell Ca^{2+}_i dynamics during prolonged ND and HFD feeding and subsequent recovery with ND. *C*: Quantifications of β-cell Ca^{2+}_i peak amplitude ($\Delta F/F_{basal\ min}$ over basal mean) in the first phase (0′–5′) after glucose injection. Dashed line represents the switching from HFD to ND. *D*: In vivo calcium efficacy of β-cells during ND or HFD, calculated by correlation of stimulated plasma insulin levels and β-cell Ca^{2+}_i dynamics and corrected for islet volume adaptation. n = 4–8 islets and mice; mean ± SEM. $^*P < 0.05$ vs. ND; $^\wedge P < 0.05$ vs. prediet. AUC, area under the curve.

observed in several models of β-cell stress and linked to altered gene expression of Ca^{2+}-channel subunits (41), impaired glucose metabolism (42), or abnormal Ca^{2+}_i handling (43). Importantly, blunted stimulated Ca^{2+}_i dynamics might be directly related to the increased basal Ca^{2+}_i, as both have been observed to occur simultaneously in pathophysiological conditions (39,44). Our observation that stimulated insulin release is elevated despite reduced Ca^{2+}_i dynamics suggests that functional compensation in HFD is accomplished by the amplifying pathway of insulin secretion and augmented calcium efficacy (45–47). This is probably mediated by free fatty acids, which rise during HFD feeding (48) and have been shown to potentiate glucose-stimulated insulin secretion (49). Mimicking HFD feeding conditions in vitro by culture of isolated islets in palmitate and slightly elevated glucose, we found Epac to be involved in amplified calcium efficacy. These findings underline the potential of lipid-derived signals to activate the amplifying pathway (50) and the role of Epac in elevated β-cell function during HFD (31).

Interestingly, islet mass expansion stopped but did not reverse after cessation of HFD feeding. However, given the observed slow adaptation of β-cell mass to the changed metabolic environment, this might take place within a longer time frame than assessed in our study. In contrast, HFD-induced alterations in glucose homeostasis and Ca^{2+}_i dynamics were quickly reversed by ND feeding. This is in agreement with the rapid recovery of mouse and human islets isolated from subjects with diabetes (51,52) and might explain diverse findings in isolated islets in vitro in comparison with the in vivo results presented here (5).

In conclusion, our data provide the first in vivo evidence that β-cell function outweighs the adaptive response of islet mass during compensation of insulin resistance and progression to prediabetes. Thereby, the amplifying pathway of insulin secretion, via increased calcium efficacy and Epac signaling, plays a crucial role in the β-cells' capacity to compensate for the higher insulin demand. At the onset of prediabetes, β-cell function is still enhanced but shows signs of weakened compensation. Whether this is primarily the result of reduced stimulated Ca^{2+}_i dynamics or of additionally decreasing calcium efficacy requires further investigation. While caution has to be used when translating mouse data to the human situation, it is likely that due to the low proliferative potential of adult human β-cells (13) the role of β-cell function in human diabetes pathogenesis will be even more significant. Thus, we believe that T2D prevention and treatment should aim at

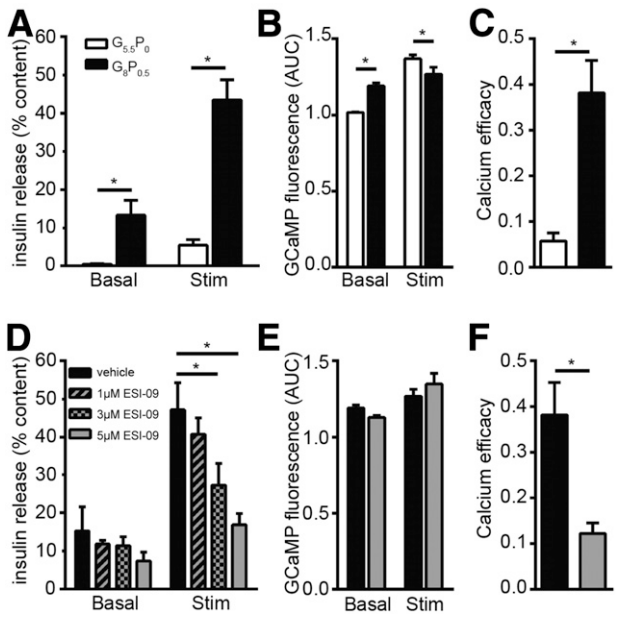

Figure 7—Palmitate-induced increased calcium efficacy in isolated islets involves Epac signaling. *A*: Basal and stimulated insulin secretion from isolated islets after 24-h culture in $G_{5.5}P_0$ or in $G_8P_{0.5}$. n = 5. *B*: β-Cell Ca^{2+}_i dynamics of Pdx1CreER-GCaMP3 islets under conditions identical to those in *A*. n = 18–21 islets from 5–6 experiments. *C*: In vitro calcium efficacy calculated from islets shown in *A* and *B*. n = 4. *D–F*: Effect of indicated concentration of the Epac-specific inhibitor ESI-09 on insulin secretion (*D*) (n = 4–5), Ca^{2+}_i dynamics (*E*) (n = 17–19 islets from 6 experiments), and calcium efficacy (*F*) (n = 4) of islets cultured for 24 h in $G_8P_{0.5}$. Mean ± SEM. $^*P < 0.05$. AUC, area under the curve.

protecting and improving β-cell function by addressing calcium dynamics and efficacy.

Acknowledgments. The authors thank Katharina Hüttner, Chrissy Kühn, Angela Hartke, Alin Pfennig, and Claudia Möx, the Paul Langerhans Institute Dresden, for excellent technical assistance.

Funding. This work was partly supported with funds from the Emmy Noether Program of the German Research Foundation (DFG) (www.dfg.de); the DFG–Center for Regenerative Therapies Dresden, Cluster of Excellence (www.crt-dresden.de); and DFG SFB/Transregio 127; and the German Ministry for Education and Research (www.bmbf.de) to the DZD and to the Competence Network Diabetes Mellitus.

Duality of Interest. This work was also supported with funds from Boehringer Ingelheim Pharma GmbH & Co. KG. No other potential conflicts of interest relevant to this article were reported.

Author Contributions. C.C. and S.S. designed the study, analyzed data, and wrote the manuscript. C.C. performed the experiments. H.C., C.M.C., J.A.C., S.R.J., J.S., and I.U. analyzed data and provided intellectual input. S.S. provided funding. S.S. is the guarantor of this work and, as such, had full access to all the data in the study and takes responsibility for the integrity of the data and the accuracy of the data analysis.

References

1. Kahn SE, Hull RL, Utzschneider KM. Mechanisms linking obesity to insulin resistance and type 2 diabetes. Nature 2006;444:840–846
2. Meigs JB, Wilson PW, Fox CS, et al. Body mass index, metabolic syndrome, and risk of type 2 diabetes or cardiovascular disease. J Clin Endocrinol Metab 2006;91:2906–2912
3. Kahn SE, Prigeon RL, McCulloch DK, et al. Quantification of the relationship between insulin sensitivity and beta-cell function in human subjects. Evidence for a hyperbolic function. Diabetes 1993;42:1663–1672
4. Kanno A, Asahara S, Masuda K, et al. Compensatory hyperinsulinemia in high-fat diet-induced obese mice is associated with enhanced insulin translation in islets. Biochem Biophys Res Commun 2015;458:681–686
5. Gonzalez A, Merino B, Marroquí L, et al. Insulin hypersecretion in islets from diet-induced hyperinsulinemic obese female mice is associated with several functional adaptations in individual β-cells. Endocrinology 2013;154:3515–3524
6. Chen C, Hosokawa H, Bumbalo LM, Leahy JL. Mechanism of compensatory hyperinsulinemia in normoglycemic insulin-resistant spontaneously hypertensive rats. Augmented enzymatic activity of glucokinase in beta-cells. J Clin Invest 1994;94:399–404
7. Hull RL, Kodama K, Utzschneider KM, Carr DB, Prigeon RL, Kahn SE. Dietary-fat-induced obesity in mice results in beta cell hyperplasia but not increased insulin release: evidence for specificity of impaired beta cell adaptation. Diabetologia 2005;48:1350–1358
8. Ahrén J, Ahrén B, Wierup N. Increased β-cell volume in mice fed a high-fat diet: a dynamic study over 12 months. Islets 2010;2:353–356
9. Mezza T, Muscogiuri G, Sorice GP, et al. Insulin resistance alters islet morphology in nondiabetic humans. Diabetes 2014;63:994–1007
10. Bonner-Weir S, Li WC, Ouziel-Yahalom L, Guo L, Weir GC, Sharma A. Beta-cell growth and regeneration: replication is only part of the story. Diabetes 2010;59:2340–2348
11. Butler AE, Janson J, Soeller WC, Butler PC. Increased beta-cell apoptosis prevents adaptive increase in beta-cell mass in mouse model of type 2 diabetes: evidence for role of islet amyloid formation rather than direct action of amyloid. Diabetes 2003;52:2304–2314
12. Rahier J, Guiot Y, Goebbels RM, Sempoux C, Henquin JC. Pancreatic beta-cell mass in European subjects with type 2 diabetes. Diabetes Obes Metab 2008;10(Suppl. 4):32–42
13. Saisho Y, Butler AE, Manesso E, Elashoff D, Rizza RA, Butler PC. β-cell mass and turnover in humans: effects of obesity and aging. Diabetes Care 2013;36:111–117
14. Hanley SC, Austin E, Assouline-Thomas B, et al. beta-Cell mass dynamics and islet cell plasticity in human type 2 diabetes. Endocrinology 2010;151:1462–1472
15. Del Guerra S, Lupi R, Marselli L, et al. Functional and molecular defects of pancreatic islets in human type 2 diabetes. Diabetes 2005;54:727–735
16. Collins SC, Hoppa MB, Walker JN, et al. Progression of diet-induced diabetes in C57BL6J mice involves functional dissociation of Ca2(+) channels from secretory vesicles. Diabetes 2010;59:1192–1201
17. Dalbøge LS, Almholt DL, Neerup TS, et al. Characterisation of age-dependent beta cell dynamics in the male db/db mice. PLoS One 2013;8:e82813
18. Finegood DT, McArthur MD, Kojwang D, et al. Beta-cell mass dynamics in Zucker diabetic fatty rats. Rosiglitazone prevents the rise in net cell death. Diabetes 2001;50:1021–1029
19. Topp BG, Atkinson LL, Finegood DT. Dynamics of insulin sensitivity, -cell function, and -cell mass during the development of diabetes in fa/fa rats. Am J Physiol Endocrinol Metab 2007;293:E1730–E1735
20. Butler AE, Janson J, Bonner-Weir S, Ritzel R, Rizza RA, Butler PC. Beta-cell deficit and increased beta-cell apoptosis in humans with type 2 diabetes. Diabetes 2003;52:102–110
21. Rahier J, Goebbels RM, Henquin JC. Cellular composition of the human diabetic pancreas. Diabetologia 1983;24:366–371
22. Hara M, Wang X, Kawamura T, et al. Transgenic mice with green fluorescent protein-labeled pancreatic beta -cells. Am J Physiol Endocrinol Metab 2003;284:E177–E183
23. Gu G, Dubauskaite J, Melton DA. Direct evidence for the pancreatic lineage: NGN3+ cells are islet progenitors and are distinct from duct progenitors. Development 2002;129:2447–2457
24. Zariwala HA, Borghuis BG, Hoogland TM, et al. A Cre-dependent GCaMP3 reporter mouse for neuronal imaging in vivo. J Neurosci 2012;32:3131–3141
25. Borg DJ, Weigelt M, Wilhelm C, et al. Mesenchymal stromal cells improve transplanted islet survival and islet function in a syngeneic mouse model. Diabetologia 2014;57:522–531
26. Chmelova H, Cohrs CM, Chouinard JA, et al. Distinct roles of β-cell mass and function during type 1 diabetes onset and remission. Diabetes 2015;64:2148–2160
27. Speier S, Nyqvist D, Köhler M, Caicedo A, Leibiger IB, Berggren PO. Noninvasive high-resolution in vivo imaging of cell biology in the anterior chamber of the mouse eye. Nat Protoc 2008;3:1278–1286
28. Speier S, Nyqvist D, Cabrera O, et al. Noninvasive in vivo imaging of pancreatic islet cell biology. Nat Med 2008;14:574–578
29. Beattie GM, Montgomery AM, Lopez AD, et al. A novel approach to increase human islet cell mass while preserving beta-cell function. Diabetes 2002;51:3435–3439
30. Marciniak A, Cohrs CM, Tsata V, et al. Using pancreas tissue slices for in situ studies of islet of Langerhans and acinar cell biology. Nat Protoc 2014;9:2809–2822
31. Song WJ, Mondal P, Li Y, Lee SE, Hussain MA. Pancreatic β-cell response to increased metabolic demand and to pharmacologic secretagogues requires EPAC2A. Diabetes 2013;62:2796–2807
32. Seino S, Takahashi H, Fujimoto W, Shibasaki T. Roles of cAMP signalling in insulin granule exocytosis. Diabetes Obes Metab 2009;11(Suppl. 4):180–188
33. Nyqvist D, Speier S, Rodriguez-Diaz R, et al. Donor islet endothelial cells in pancreatic islet revascularization. Diabetes 2011;60:2571–2577
34. Rodriguez-Diaz R, Speier S, Molano RD, et al. Noninvasive in vivo model demonstrating the effects of autonomic innervation on pancreatic islet function. Proc Natl Acad Sci U S A 2012;109:21456–21461
35. Ilegems E, Dicker A, Speier S, et al. Reporter islets in the eye reveal the plasticity of the endocrine pancreas. Proc Natl Acad Sci U S A 2013;110:20581–20586
36. Winzell MS, Ahrén B. The high-fat diet-fed mouse: a model for studying mechanisms and treatment of impaired glucose tolerance and type 2 diabetes. Diabetes 2004;53(Suppl. 3):S215–S219

37. Rosengren AH, Braun M, Mahdi T, et al. Reduced insulin exocytosis in human pancreatic β-cells with gene variants linked to type 2 diabetes. Diabetes 2012;61:1726–1733
38. Matveyenko AV, Butler PC. Relationship between beta-cell mass and diabetes onset. Diabetes Obes Metab 2008;10(Suppl. 4):23–31
39. Do OH, Low JT, Gaisano HY, Thorn P. The secretory deficit in islets from db/db mice is mainly due to a loss of responding beta cells. Diabetologia 2014;57:1400–1409
40. Itoh Y, Kawamata Y, Harada M, et al. Free fatty acids regulate insulin secretion from pancreatic beta cells through GPR40. Nature 2003;422:173–176
41. Roe MW, Worley JF 3rd, Tokuyama Y, et al. NIDDM is associated with loss of pancreatic beta-cell L-type Ca2+ channel activity. Am J Physiol 1996;270:E133–E140
42. Kato S, Ishida H, Tsuura Y, et al. Alterations in basal and glucose-stimulated voltage-dependent Ca2+ channel activities in pancreatic beta cells of non-insulin-dependent diabetes mellitus GK rats. J Clin Invest 1996;97:2417–2425
43. Marie JC, Bailbé D, Gylfe E, Portha B. Defective glucose-dependent cytosolic Ca2+ handling in islets of GK and nSTZ rat models of type 2 diabetes. J Endocrinol 2001;169:169–176
44. Khaldi MZ, Guiot Y, Gilon P, Henquin JC, Jonas JC. Increased glucose sensitivity of both triggering and amplifying pathways of insulin secretion in rat islets cultured for 1 wk in high glucose. Am J Physiol Endocrinol Metab 2004;287:E207–E217
45. Ammälä C, Ashcroft FM, Rorsman P. Calcium-independent potentiation of insulin release by cyclic AMP in single beta-cells. Nature 1993;363:356–358
46. Sato Y, Anello M, Henquin JC. Glucose regulation of insulin secretion independent of the opening or closure of adenosine triphosphate-sensitive K+ channels in beta cells. Endocrinology 1999;140:2252–2257
47. Ha J, Satin LS, Sherman AS. A mathematical model of the pathogenesis, prevention, and reversal of type 2 diabetes. Endocrinology 2016;157:624–635
48. Ahrén B, Scheurink AJ. Marked hyperleptinemia after high-fat diet associated with severe glucose intolerance in mice. Eur J Endocrinol 1998;139:461–467
49. Dobbins RL, Chester MW, Stevenson BE, Daniels MB, Stein DT, McGarry JD. A fatty acid- dependent step is critically important for both glucose- and non-glucose-stimulated insulin secretion. J Clin Invest 1998;101:2370–2376
50. Nolan CJ, Madiraju MS, Delghingaro-Augusto V, Peyot ML, Prentki M. Fatty acid signaling in the beta-cell and insulin secretion. Diabetes 2006;55(Suppl. 2):S16–S23
51. Alarcon C, Boland BB, Uchizono Y, et al. Pancreatic β-cell adaptive plasticity in obesity increases insulin production but adversely affects secretory function. Diabetes 2016;65:438–450
52. Henquin JC, Dufrane D, Kerr-Conte J, Nenquin M. Dynamics of glucose-induced insulin secretion in normal human islets. Am J Physiol Endocrinol Metab 2015;309:E640–E650